Astronomy & Astrophysics manuscript no.
(will be inserted by hand later)

Diagnostics of SS433 with the RXTE

Filippova E.[1,2], Revnivtsev M.[1,2], Fabrika S.[3], Postnov K.[4], Seifina E.[4]

[1] Max-Planck-Institute für Astrophysik, Karl-Schwarzschild-Str. 1, D-85740 Garching bei München, Germany
[2] Space Research Institute, Russian Academy of Sciences, Profsoyuznaya 84/32, 117997 Moscow, Russia
[3] Special Astrophysical Observatory, Nizhnij Arkhyz, Karachaevo-Cherkesiya, 369167, Russia
[4] Sternberg Astronomical Institute, 119992, Moscow, Russia

Abstract. We present analysis of extensive monitoring of SS433 by the RXTE observatory collected over the period 1996-2005. The difference between energy spectra taken at different precessional and orbital phases shows the presence of a strong photoabsorption ($N_{\rm H} > 10^{23}$ **cm**$^{-2}$) near the optical star, probably due to its powerful dense wind. Assuming that a precessing accretion disk **is thick**, we recover the temperature profile in the X-ray emitting jet that best fits the observed precessional variations of the X-ray emission temperature. The hottest visible part of the X-ray jet is located at a distance of $l_0/a \sim 0.06 - 0.09$, or $\sim 2 - 3 \times 10^{11}$cm from the central compact object and has a temperature of about $T_{\rm max} \sim 30$ keV. We discovered appreciable orbital X-ray eclipses at the "crossover" precessional phases (jets are in the plane of the sky, disk is edge-on) which put a lower limit on the size of the optical component $R/a \gtrsim 0.5$ and an upper limit on a mass ratio of binary companions $q = M_{\rm x}/M_{\rm opt} \lesssim 0.3 - 0.35$, **assuming that the radius of the eclipsing region can not be much larger than** $1.2R_{\rm Roche,secondary}$**.** The size of the eclipsing region can be larger than secondary's Roche lobe because of substantial photoabsorption by dense stellar wind. This must be taken into account when evaluating the mass ratio from analysis of X-ray eclipses.

Key words. accretion, accretion disks– black hole physics – instabilities – stars:binaries:general – X-rays: general – X-rays: stars

1. Introduction

SS433 is the only Galactic X-ray binary with X-ray emission from optically thin thermal plasma originating in hot jets outflowing with a sub-relativistic velocity of 0.26 c. The binary system is thought to consist of a compact object (probably, a black hole) accreting matter at a super-Eddington rate from a high-mass star filling its Roche lobe (Margon 1984, Cherepaschuk 2002, see Fabrika 2004 for a recent review).

Apparently, the innermost accretion flow and the supercritical accretion disk wind completely screen the region of the main energy release and most of the energy from SS433 is observed in the optical and UV (Cherepashchuk et al., 1982; Dolan et al., 1997).

The system demonstrates a complex variability including periodicities - the precessional (∼162 days), orbital (∼13 days), and nutational (**nodding**,∼ 6 days) periods - which can be used to tightly constrain the binary system parameters. In particular, the kinematical model of the system yields the binary inclination angle is $i \sim 78.05°$ and the jet precession angle is $\sim 20.92°$ Fabrika (2004).

Send offprint requests to: kate@hea.iki.rssi.ru

Mildly relativistic ($v \sim 0.26$c) jets launched in the vicinity of the compact object consist of protons and electrons ("heavy" jet) with a high temperature (1-30 keV). Plasma moving along the jet gradually cools down so that at distances $\sim 10^{13} - 10^{14}$ cm from the central object thermal instability develops and clumps start forming. At distances $10^{14} - 10^{15}$ cm the temperature of matter drops to $\sim 2 \times 10^4$K so that optical line emission appears. At larger distances the jets shine in the radio diapason.

The main properties of the X-ray emission observed from SS433 can be summarized as follows:

- The X-ray emission mechanism is thermal bremsstrahlung radiation (e.g. Marshall et al. 1979; Watson et al. 1986; Matsuoka, Takano, & Makishima 1986; Brinkmann et al. 1991).
- The temperature of optically thin plasma decreases along the jet. The hottest regions near the jet base have temperatures up to ∼**20-**30 keV (e.g. Kotani et al. 1996; Marshall, Canizares, & Schulz 2002; Cherepashchuk et al. 2003; Namiki et al. 2003).
- A detailed study of X-ray emission lines in SS433 shows that the **full** opening angle of the jet should be very small, not larger than $\sim 1 - 2°$. Such an opening angle roughly corresponds to free expansion of the jet

material in the direction perpendicular to the jet motion (Marshall, Canizares, & Schulz 2002; Namiki et al. 2003).
– There are X-ray eclipses caused by the **donor** star. The temperature of the observed radiation significantly drops during the eclipse, the depth of the eclipse increases at high energies (Stewart et al. 1987; Kawai et al. 1989; Brinkmann et al. 1991).
– Precession of the geometrically thick accretion disk is accompanied by strong variations in both temperature and flux of X-ray emission (Yuan et al. 1995). Amplitudes of precessional and orbital variations of X-ray emission strongly increase with energy (e.g. Cherepashchuk et al. 2005). The precession variations are likely to be due to partial eclipse of the X-ray jets by the thick precessing accretion disk.

Over the life time of the RXTE observatory a lot of observations of SS433 were performed at different precessional and orbital phases (see e.g. **Gies et al. 2002; Nandi et al. 2005**). The relatively complete sampling of the source at different orbital and precessional phases provides us an opportunity to perform a tomographic study of the X-ray jet in SS433. The examination of orbital eclipses (caused by the optical star) and precessional variability (caused by the thick accretion disk) allows contributions from different parts of the jet to the total X-ray emission to be separated.

2. Observations and data analysis

In the present paper, we have used all publicly available data of the RXTE observatory obtained from April 1996 until August 2004 and also the results of our dedicated SS433 observations during RXTE AO10 (P91103). In total, this includes 100 observations taken at different precessional and orbital phases of the system. We have used precessional and orbital ephemeris furnished by Fabrika (2004). While analyzing the observed X-ray flux variations we adopted the following parameters: the moment of the maximum emission line separation (T3) $T_3 = 2443507.47$ JD, the precessional period $P_{\rm prec} = 162.375$ days, the orbital period $P_{\rm orb} = 13.08211$ days, the moment of the primary optical eclipse $T_0 = 2450023.62$ JD. To treat nutational variations, we adopted $P_{\rm nut} = 6.2877$ days, the moment of maximum brightness in V band due to **the** nodding variability $T_{0,\rm nut} = 2450000.94$ JD, the nodding amplitude 2.8°.

Standard tasks of the LHEASOFT/FTOOLS 5.3.1 package were utilized for data processing. For accurate background modeling of the PCA spectrometer of the RXTE observatory we applied the "L7_240CM" faint model. Only spectra obtained by the PCU2 detector have been selected. To construct broad-band spectra, data from HEXTE detectors have also been used.

3. Variation of X-ray emission over precessional and orbital periods

The binary system is schematically shown in Fig.1. The binary separation is assumed to be $a \sim 4 \times 10^{12}$ cm (e.g. Hillwig et al. 2004). The mass ratio of the companions is still not well constrained and varies in different works from $q = M_{\rm x}/M_{\rm opt} \sim 0.2$ to $q \sim 0.6$ (Antokhina, Seifina, & Cherepashchuk 1992; Gies, Huang, & McSwain 2002). However the latest studies of the kinematics of the binary system favor a smaller mass ratio $q \sim 0.2 - 0.3$ **(Hillwig et al. 2004; Cherepashchuk et al. 2005)**.

After discovery of the donor star absorption spectrum in the blue spectral region of SS433 (Gies, Huang, & McSwain 2002), there were several contradictory results on the orbital behaviour of the absorption lines. From our experience (Cherepashchuk et al. 2005) in spectral study of these absorption lines we may conclude that there are two important restriction, adhering to which one may hope to detect "real donor star" absorption lines. 1. Observations must be performing in the precessional phases of the most open accretion disk ($\psi \sim 0$), when the disk outflow does not intersect the line of sight. The observations by Gies, Huang, & McSwain (2002); Hillwig et al. (2004); Cherepashchuk et al. (2005) satisfy to this condition. 2. Only weakest absorption lines have to be taken into account, stronger lines will trace the gas streams in the binary even at precessional phases $\psi \sim 0$, because of the huge ($\sim 10^{-4} M_\odot$/yr) mass transfer rate in SS433 (Fabrika 2004). In the commonly used cross-correlation method the strongest Fe II absorption lines in the studied spectral region will dominate and distort the radial velocity curves (Hillwig et al. 2004; Barnes et al. 2006). The observations by Gies, Huang, & McSwain (2002); Cherepashchuk et al. (2005) satisfy to the second restriction. The great care must be taken when deriving and interpreting the behaviour of these absorption features (Barnes et al. 2006). The heating of the donor surface revealed by Cherepashchuk et al. (2005) makes the task even more complicated.

In SS433, the optical star loses matter both via **the Roche lobe overflow and a strong stellar wind**. Matter which goes through the inner Lagrangian point forms an accretion disk around the compact object which eventually becomes geometrically thick because of strongly super-Eddington accretion (Abramowicz (2004) and references therein) . Both simple estimates and more detailed calculations show that this geometrically thick accretion disk should have height comparable to its radius $H/R \sim 1$ (e.g. Okuda et al. 2005; Nazarenko & Glazunova 2005).

Observational appearance of SS433 in X-rays is determined by multi-temperature optically thin thermal plasma emission of the jet. The X-ray emission from SS433

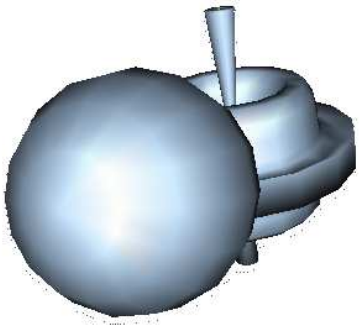

Fig. 1. Scheme of the X-ray binary SS433. Both the optical component and geometrically thick accretion disk can eclipse central parts of the X-ray jet.

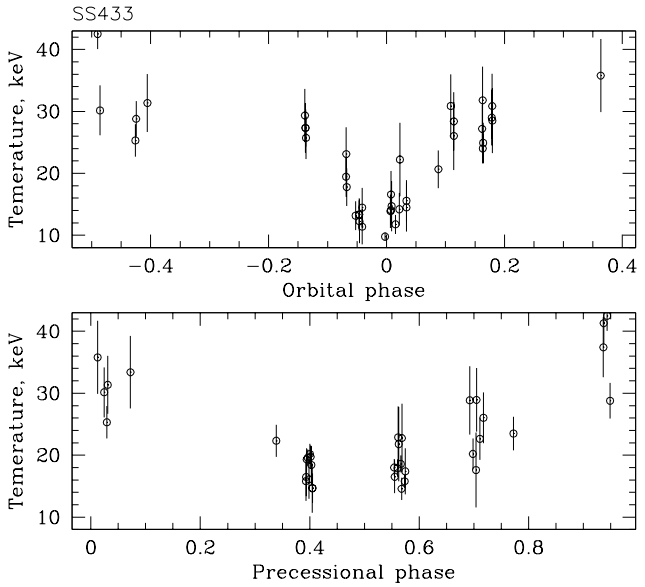

Fig. 2. The temperature of optically thin thermal plasma (bremsstrahlung fit to the 10-25 keV RXTE/PCA data) emission observed from SS433 as a function of orbital and precessional phases.

is subjected to both systematic and chaotic variations. Chaotic variations are likely caused by self-similar variability in the instantaneous mass accretion rate in the disk (Revnivtsev et al. 2005). Systematic variations of X-ray luminosity and spectral shape are determined by precessional (phases ψ) and orbital (phases ϕ) motions in the binary system.

Orbital variations are not strong, except for the eclipse. In contrast, the precessional variations are much more pronounced. In order to demonstrate this, in Fig. 2 we plot the temperature of the X-ray emission as a function of precessional and orbital phases. As the X-ray emission of SS433 is essentially multi-temperature we considered only high energy part of the spectrum (10-25 keV) that probes the hottest, innermost regions of X-ray jet. The presented temperatures are best fit parameters of the bremsstrahlung model describing the observed spectra of SS433 in the 10-25 keV band. To demonstrate orbital variations, we have chosen the precessional periods interval $\psi = [-0.06, 0.06]$ (the maximum disk opening phase). For precessional variations only orbital phases $\phi = [0.3, 0.7]$ (the off-eclipse phases) have been selected.

Broad-band X-ray spectra of SS433 at different precessional phases are shown in Fig.3

It is seen that the best fit temperature does not exhibit any correlation with the orbital phase except the X-ray eclipse (from $\phi \sim -0.15$ to $\phi \sim 0.15$) while strongly correlates with the precessional phase.

Note that even at very close **both** precessional and orbital phases there are statistically significant differences in the maximum jet temperatures. Such temperature variations could be caused either by the nodding motion of the geometrically thick accretion disk or by chaotic (red noise) variations of the physical parameters of the jet plasma, similar to red-noise variations observed in the integrated X-ray flux (Revnivtsev et al. 2005).

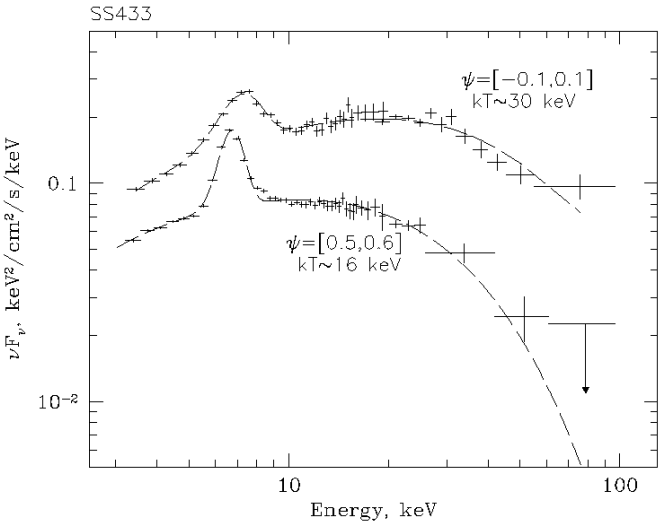

Fig. 3. Typical spectra of SS433 taken at two different disk precession phases. Only off-eclipse orbital phases $\phi = [0.3 - 0.7]$ are selected for this plot. The dashed curves show the fit by bremsstrahlung model **with broad gaussian line profile**. The best fit values of temperature of optically thin plasma are quoted.

4. The inner jet tomography by orbital and precessional eclipses

The precessional motion of the geometrically thick accretion disk causes obscuration of the jets. The upper jet (see Fig.1) is least eclipsed near the precessional phase $\psi = 0.0$ (i.e. at the maximum disk opening when the upper jet points towards the observer) and is most eclipsed at $\psi = 0.5$ (i.e. when the upper jet points away from the observer). Between precessional phases $\psi \sim 0.33$

and $\psi \sim 0.66$ (the disk "edge-on" or "crossover" phases), it is the opposite (lower) jet that starts dominating the X-ray emission because at these phases it is directed towards the observer.

The jet eclipses by the optical star and/or accretion disk leads to temperature variations of the observed X-ray emission. Thus, by examining differences between spectra taken during eclipses and off eclipses we can find the spectral contribution from the innermost (the hottest) regions of the jet.

In Fig. 4 we present two spectra of the jet in SS433. In the left panel (a), we plot the difference between spectra taken during the primary eclipse at $\phi = 0.021$ MJD 53581.89 and immediately after the eclipse at $\phi = 0.114$ MJD 53582.94 (open circles) together with off-eclipse spectrum at $\phi = 0.114$ (crosses). The spectra were accumulated over the 1024-s period. The precessional phase at that time was $\psi \sim 0$.

In the right panel (b), we show the difference between spectra taken at precessional phases $\psi = 0$ (MJD 53076.85) and $\psi = 0.4$ (MJD 50878.98)[1]. The curves show best-fit bremsstrahlung plus photoabsorption models to the data in the 3-5 and 11-25 keV bands where powerful emission lines do not contribute significantly. The dotted curves show bremsstrahlung models with a conventional photoabsorption column density of $\mathbf{N}_{\rm H} = 10^{22}$ cm^{-2} (e.g Kawai et al. 1989).

The high energy parts (11-25 keV) of the "differential" and integral spectra of SS433 are almost identical because they both are mainly determined by emission from the hottest parts of the jet. However, a strong photoabsorption is observed near the orbital eclipse (the left panel of Fig.4). The best-fit value of the absorption column density in this spectrum is $\mathbf{N}_{\rm H} = (12.5 \pm 1.5) \times 10^{22}$ cm^{-2}, much higher than the conventional value.

The spectrum of the hottest (innermost) part of the jet as derived from precessional variations off the primary eclipse (the right panel of Fig.4) also suggests some photoabsorption, but of considerably smaller value – here the best-fit absorbing column density is $\mathbf{N}_{\rm H} = (4.5 \pm 1.5) \times 10^{22}$ cm^{-2}.

So the "differential" X-ray spectra of SS433 indicate the presence of an absorbing material in the SS433 binary system manifesting itself as a strong photoabsorption of X-ray emission from the innermost parts of the jet. In regions close to the companion star the density of such an absorbing material is much higher – the column density along the line of sight at these phases becomes almost Compton thick ($\mathbf{N}_{\rm H} > 10^{23}$ cm^{-2}). Note that signatures of absorbing material near the optical star have previously been obtained from studies of optical absorption lines (Fabrika 1997; Fabrika et al. 1997). These studies revealed a significant strengthening in blue-shifted absorption components of P Cyg-like line profiles at orbital phases close to the primary eclipse.

The presence of such a dense absorbing material can be a signature of powerful winds from the optical supergiant star and super-Eddington accretion disk, as well as of the wind-star interaction. **For the plasma with solar abundance it becomes almost opaque for X-rays when $N_H = 10^{24} cm^{-2}$.**

Assuming the mass-loss rate in the disk wind $\dot{M} \sim 10^{-5} M_\odot$/yr and the line-of-sight wind velocity in this precessional phase $V_{disk\ wind} \sim 1000\ km/s$ (Fabrika 1997) we can roughly estimate the column density of the disk wind close to the donor $N_H \sim \dot{M}/4a\mu m_p V_{disk\ wind} \sim 1 \cdot 10^{23}\ cm^{-2}$.

In order to estimate the possible increase of the eclipsing region radius due to the donor stellar wind we adopted the single A supergiant model for the star and took parameters of the stellar wind (its mass loss rate and terminal velocity) from the work of Achmad et al. (1997). From observations and theoretical models follow that the mass loss rate of A supergiant strongly depends on the mass of the star and its effective temperature and varies from $\sim 10^{-9} M_\odot/yr$ up to $\sim 10^{-6} M_\odot/yr$. The observed values of the terminal velocity lie in the range 120 - 200 km/s. For the velocity law we use formula

$$v(r) = v_\infty (1 - R_{star}/r)^\beta$$

where $\beta = 0.8$ (Achmad et al. 1997), v_∞ - the wind terminal velocity, R_{star} - star radius, r - distance from the companion star. And from the mass conservation law follows the formula for wind density n(r):

$$n(r) = \frac{n_0 (1 - R_{star}/r)^\beta}{(r/a)^2 (1 - R_{star}/r)^\beta}$$

where n_0 is the number density at the distance a. As the spectral type and mass of the optical star aren't exactly defined we consider several cases and obtained following results. For maximal observed value of $\dot{M} = 8 \times 10^{-7} M_\odot/yr$ (for star type A1 Iae, Achmad et al. 1997) the stellar wind will increase the size of the star up to 10 %. The maximal theoretical value $\dot{M} = 10^{-6} M_\odot/yr$ can increase the size of the star up to 20 %.

So the dense wind should effectively increase the "size" of the star as inferred from X-ray **and may be even from optical** eclipses. So measurements of the Roche lobe of the secondary in SS433 from orbital X-ray eclipse only may be significantly overestimated due to photoabsorption in the wind and cannot be used to constrain the mass ratio in this binary system without additional model assumptions.

Note that the photoabsorption we discussed above should not be visible in the integrated spectrum of SS433 averaged over the entire eclipse (or **separately** ingress

[1] These two observations were performed during different high-voltage epoch of the PCA. We recalculated them to a single response matrix. Both spectra were taken off the orbital eclipses

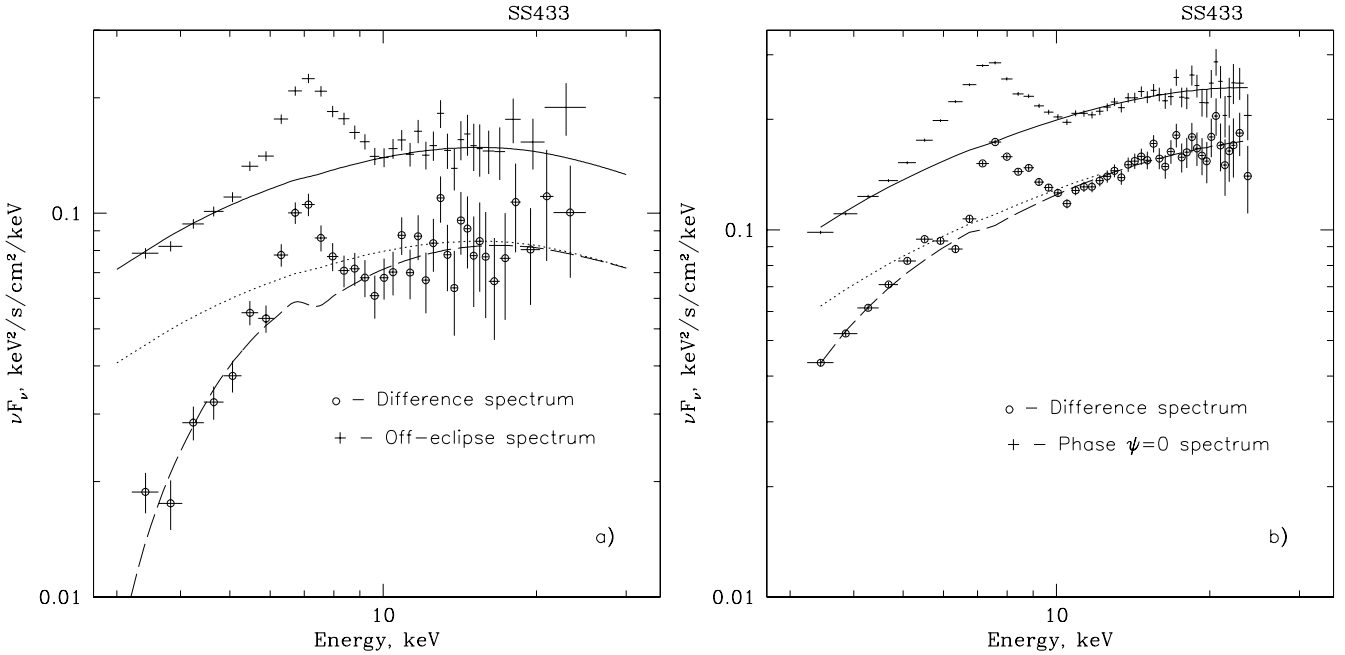

Fig. 4. a) The X-ray spectrum of SS433 immediately after the eclipse (the orbital phase $\phi = 0.114$, crosses) and the spectrum from the inner part of the jet obtained by subtracting the spectrum taken at $\phi = 0.021$ from that at $\phi = 0.114$. b) The X-ray spectrum of SS433 at precessional phase $\psi \sim 0$ and difference between this spectrum and that at $\psi \sim 0.4$ (both spectra were collected over off-eclipse orbital phases). Solid curves show thermal bremsstrahlung models with photoabsorption fitted to the data in the 3-5 and 11-25 keV bands. Dotted curves show best-fit bremsstrahlung models to the "differential" spectra with a nominal photoabsorption column density of $N_{\rm H} = 10^{22}$ cm^{-2}.

to and egress out of the eclipse) because only emission from the hottest innermost parts of the jet are screened/absorbed, while outer cooler parts of the jet, which dominate emission at energies $< 3 - 5$ keV where the RXTE spectra are most sensitive to absorption, are located much farther away from the star and hence X-ray emission from these parts are virtually unabsorbed.

5. Jet eclipses by the thick disk

Eclipses of the X-ray jet by thick disk is a geometrical effect and depends only on the orientation of the disk changing with the precessional phase. Therefore, assuming some reasonable geometry of the thick disk, observations of SS433 at different precessional phases can be used to derive emission parameter profiles along the jet.

5.1. The structure of jets

We consider the jets in SS433 as conical plasma flows with constant velocity $v_j = 0.26\,c$ along the jet axis. In the direction perpendicular to the jet axis the matter move with a constant velocity. We assume that the jet is uniform in the direction perpendicular to the jet axis.

The plasma flow forms a cone with constant opening angle $\mathbf{2}\theta$. Radius of the jet cross section is $r = r_b + \theta l$, where r_b is the radius of the jet near the compact object [2], l is the distance from the compact object along jet axis. The value of the cone **half-**opening angle $\theta = 0.61^\circ$ is taken from (Marshall, Canizares, & Schulz 2002).

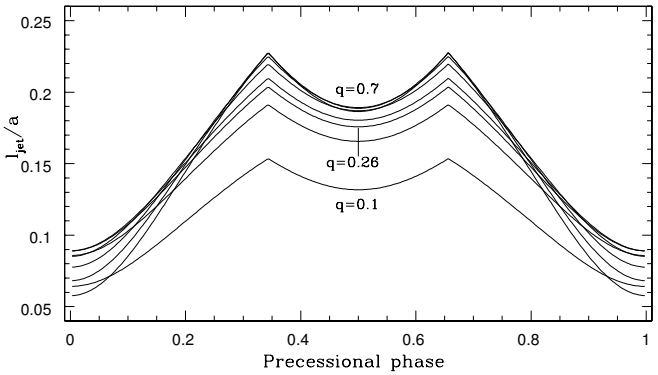

Fig. 5. The length of the invisible (eclipsed **by the disk**) part of the jet as a function of the precessional phase for q=0.1 – 0.7.

The jet plasma cools due to adiabatic expansion and radiation losses. When radiation losses become the dominant mechanism of plasma cooling, thermal instability develops. Then the temperature starts decreasing much more rapidly than in the case of purely adiabatic expansion (e.g. Brinkmann et al. 1991). Analysis of the 0.5-10 keV X-

[2] This analytical description does not mean that the jet should start near the compact object.

ray emission observed by *Chandra* from SS433 with high energy resolution suggests that such instability does not develop at least until the temperature of the plasma exceeds $kT \sim 0.5$ keV (Marshall, Canizares, & Schulz 2002). Therefore we assume that the dominant cooling process in our case (especially in the hottest parts of the jet of interest here) is adiabatic cooling and we can write:

$$\frac{3}{2}\frac{dT}{T} = \frac{dV}{V} = -\frac{2dr}{r}\,.$$

For adiabatically cooling plasma moving with constant jet opening angle the plasma temperature T changes with distance from the compact object l as:

$$\frac{T}{T_0} = (1 + \theta\frac{(l - l_0)}{r_0})^{-4/3}, \qquad (1)$$

where T_0 is the plasma temperature and r_0 is the jet cross section radius at some distance l_0 from the central source **(see also Koval' & Shakura (1989); Brinkmann et al. (1991); Kotani et al. (1996))**.

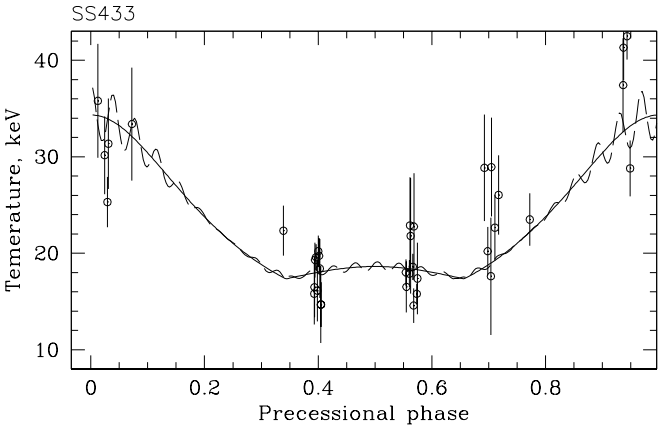

Fig. 6. The plasma temperature as a function of the precessional phase. The solid curve shows the model of adiabatic cooling of plasma moving within the cone with constant opening angle. The dashed curve shows the same model but with nodding motion of thick accretion disk included.

5.2. Precession of the geometrically thick disk

The Roche lobe only loosely constrains the accretion disk radius. For a disk lying in the orbital plane one usually adopts Paczynsky's tidal truncation radius as a measure of the outer disk radius. The accretion disk in SS433 is tilted to the orbital plane and precesses, so its outer radius can differ from Paczynsky's estimate. However, according to some numerical models (e.g. Nazarenko & Glazunova 2005), this difference is not significant, so it will be sufficient for our purposes to adopt the disk truncation radius given by Paczynski (1977):

$$\frac{R_{\rm disk}}{a} = 0.112 + \frac{0.27}{(1+q^{-1})} + \frac{0.239}{(1+q^{-1})^2}\,.$$

For geometrically thick disk ($H/R \sim 1$) and with the understanding that it should not oversize the Roche lobe of the compact star we find

$$H_{\rm disk} \lesssim (R^2_{\rm RocheBH} - R^2_{\rm disk})^{1/2}\,,$$

where the formula for $R_{\rm RocheBH}$ is adopted from Eggleton 1983):

$$\frac{R_{\rm RocheBH}}{a} = \frac{0.49q^{2/3}}{0.6q^{2/3} + \ln(1+q^{1/3})}\,.$$

In Fig. 5 we plot the distance of the nearest visible jet points from the central source as a function of the disk precessional phase for different binary mass ratios q. The mass ratio is still debatable on different grounds **(see discussion above)**, so in the present study we have varied the value of q in the range $0.2 - 0.7$.

Using the formula (1), for given parameters $q, H_{\rm disk}$ and $R_{\rm disk}$ we can calculate the maximum **model** temperature of the jet visible at different precessional phases. Note that at precessional phase intervals [0,0.33] and [0.33,0.66] the maximum emission is provided by different jets (upper or lower). Here and below all detectable parameters are calculated in the observer's reference frame, while physical parameters of the jet are given in the jet rest frame.

Comparison of the highest visible temperature profiles derived above with observational data enables us to find the model parameters (see Fig.2). The best-fit parameters of our model referred to the distance from the black hole $l_0/a = 0.06 - 0.09$ (depending on the assumed value of q) are: the highest temperature of the jet $T_0 = 30 \pm 2$ keV, the radius of the jet $r_0/a = (1 - 1.6) \times 10^{-2}$ for the jet opening angle $\theta = 0.61°$. The best-fit model is shown in Fig.6. The limited accuracy of the temperature measurements and incomplete coverage of the precessional period by observations preclude us from implementing the disk nodding motion in our model. For illustrative purposes, in Fig.6 we show the effect of the nutational variability by the dashed curve.

6. Eclipses by the optical companion

X-ray orbital eclipses observed in SS433 are widely used to constrain the geometry of the binary system (e.g. Stewart et al. 1987; Kawai et al. 1989).

Analysis of X-ray eclipses observed at the disk maximum opening (the precessional phases $\psi \sim 0.0$) allows us to get the lower **limit** on the component mass ratio in SS433 independently of (still controversial) radial velocity measurements provided by optical spectroscopy. Indeed, assuming the jet to be infinitely thin in comparison with the optical star, the duration of the X-ray eclipse yields only an upper limit on the size of the optical star (see discussion above).

On the other hand, the examination of X-ray eclipses observed at the disk "edge-on" precessional phases $\psi \sim 0.33$ or $\psi \sim 0.66$ (the so called "crossover", when the radial velocities of both jets are equal and jets exactly lie

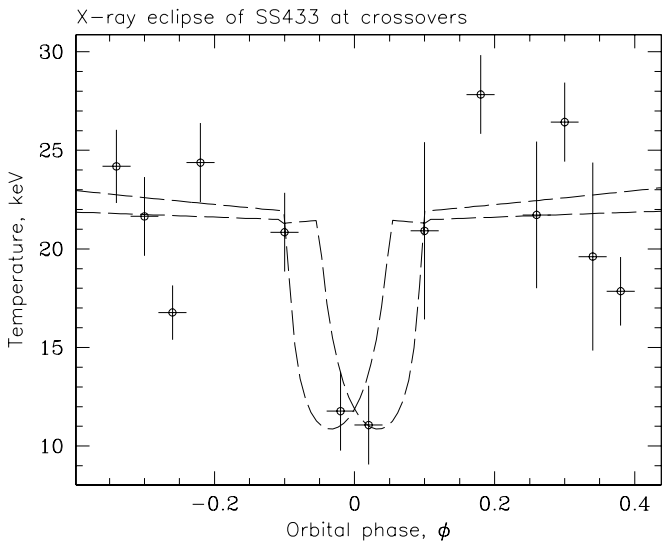

Fig. 7. Orbital X-ray eclipse of SS433 observed during the "crossover" precessional phases $|\psi - 0.33| < 0.07$ and $|\psi - 0.66| < 0.07$. Dashed lines show temperature profiles obtained in our model.

in the plane of the sky) **gives us an estimate of the** star radius **comparing with the disk thickness** . For orbital X-ray eclipses to exist, the projection of the star on the plane of the sky should not be embedded by the projected image of the thick disk. Potentially this gives us an upper limit on the value of q.

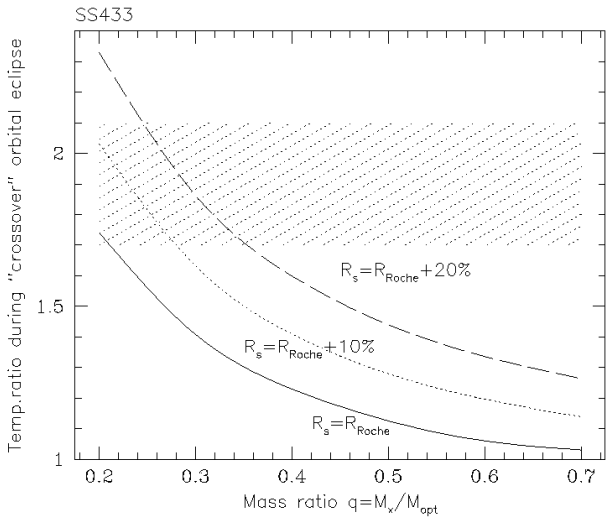

Fig. 8. The ratio of the maximum visible jet temperatures during the orbital eclipse in the "crossover" precessional phases $\psi \sim 0.33, 0.66$ as a function of the mass ratio q. The solid line is obtained for the star exactly filling its Roche lobe $R = R_{\rm Roche}$, while the dotted and dashed lines show the model with the 10% and 20% oversized star, respectively. The hatched area shows the observational constrains on the temperature ratio.

6.1. The "crossover" X-ray eclipses

In Fig.7 we present the profile of the maximum X-ray temperature measured in the orbital eclipse near precessional phases $\psi \sim 0.33, 0.66$. Observations with $\Delta\psi = \pm 0.07$ around phases of the exact "crossover" were selected. The orbital X-ray eclipse is clearly visible and shows an appreciable depth. The ratio of the maximum jet temperature derived from off-eclipse observations to that of the eclipsed jet is $\sim 1.9 \pm 0.2$. Dashed lines in the figure show examples of the jet maximum visible temperature in the eclipse at precessional phases $\psi = 0.33$ and $\psi = 0.66$ obtained in our model. The temperature profile along the jet was taken as derived in the previous section. The mass ratio $q = 0.2$ was **adopted here for clarity, and also we assumed that size of the star was 10 % larger than its Roche lobe**. We have not attempted to best fit the observed points as they were collected during different observations performed at different nutational and precessional phases.

Note that the model X-ray eclipse profiles during crossovers are not symmetric. This happens because the jets in these two cases are inclined differently with respect to the binary orbital plane.

The ratio of the maximum jet temperatures in the eclipse and off the eclipse is plotted in Fig.8 as a function of the binary mass ratio q. The solid curve shows the ratio obtained under the assumption that the size of the star equals to the volume averaged radius of the Roche lobe. The value of q affects the depth of the "crossover" eclipse via the size (thickness) of the accretion disk and the secondary star.

We have shown in Section 4 that taking the Roche lobe as a measure of the optical star size could be not fully correct estimate of the shadowing region during the orbital eclipse. The innermost parts of dense stellar wind also can absorb X-rays thus increasing the duration and depth of the X-ray eclipse. So in Fig. 8 we also plot by the dotted and dashed curves the model ratio of maximum jet temperatures in- and out- of the eclipse assuming the star radius to be $R = 1.1 R_{\rm Roche}$ and $R = 1.2 R_{\rm Roche}$ correspondingly **(see discussion in the section 4)**.

From Fig.8 we can conclude that the binary mass ratio in SS433 **can not be directly determined from the depth or duration of the X-ray eclipses. The result depends on the eclipsing region extent over the stellar Roche lobe. However, if the binary mass ratio is significantly lager than $q \sim 0.3 - 0.35$, the eclipsing region size seems to be too big, $R > 1.2 R_{\rm Roche}$. We find from our modeling that the** radius of the star (i.e. the radius of the X-ray eclipsing region which can exceed the actual star radius) should be larger than $R/a \gtrsim 0.5 - 0.55$.

6.2. X-ray eclipse at $\psi \sim 0$

To obtain a high quality profile of the jet maximum temperature across a single eclipse, we performed a set of ded-

icated RXTE observations of SS433 on July 28 – Aug. 3, 2005 near the precessional phase $\psi \sim 0$. The temperature profile found from these observations is presented in Fig.9.

Using the temperature distribution along the jet length l derived in the previous section, we calculated the expected behaviour of the maximum jet temperature during the eclipse for different sizes of the eclipsing region R with the understanding that R can be larger than the volume averaged radius of the Roche lobe of the secondary.

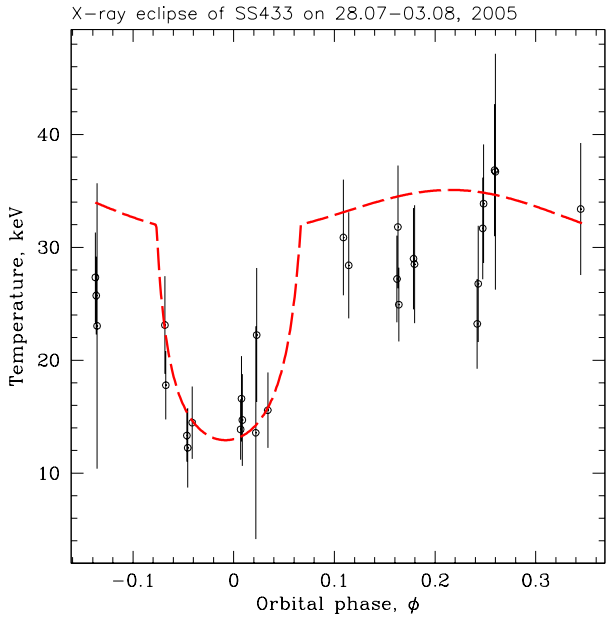

Fig. 9. The jets eclipse profile by the optical companion for $q = 0.26$. The dashed line shows the best-fit model.

The comparison with observations yielded the best-fit value $R/a = 0.53 \pm 0.02$ ($\chi^2 = 34$ for **24** degrees of freedom) for $q = 0.26$, which is ∼7% higher than size of the Roche lobe of the secondary would have at such q. The best-fit model is shown in Fig.9. For demonstration purposes we included the accretion disk nodding motion in the model shown in Fig. 9. No fitting has been attempted when nodding motion of the disk is included.

It is interesting to note that the quality of the fit can be improved if we assume non-spherical shape of the eclipsing region (star plus inner wind). This is a plausible geometry if the wind density from equatorial regions of the star is higher than from polar regions.

7. Conclusion

X-ray emission of SS433 demonstrates both chaotic (aperiodic) and periodic variations. In this paper, using extensive observational data obtained by RXTE, we studied systematic variations of X-ray emission of SS433 caused by precessional and orbital motions in the system.

– By comparing X-ray spectra of SS433 near and in the eclipse we obtained strong signatures of a significant ($N_H > 10^{23}$ cm^{-2}) photoabsorption of X-rays near the companion star. We argue that this may be due to the presence of a dense stellar wind from the companion star filling its Roche lobe. The mass loss rate in the wind which is needed to explain the observed photoabsorption is $\dot{M} \sim 10^{-6}$ M$_\odot$/yr.
– Assuming the shape of the geometrically thick accretion disk restricted by the Roche lobe size of the compact star and using the RXTE observations of SS433 at different precessional phases, we recovered the temperature profile of plasma along the jet and estimated the jet cross section at its basement. The maximum visible temperature is found to be $T \sim 30$ keV at a distance of $l/a = 0.06 - 0.09$ from the compact object. The radius of the jet at this distance is $r_0/a = 0.01 - 0.016$ for jets with constant cone open angle.
– We reliably detected orbital eclipses in the RXTE/PCA observations of SS433 during the "crossover" precessional phases when the X-ray jets and the axis of the accretion disk lie exactly in the plane of the sky. The observed depth of the X-ray eclipse implies that the size of the star is larger than $R/a \gtrsim 0.5$, yielding an upper bound on the mass ratio of the components in SS433 $q < 0.3 - 0.35$ assuming that the radius of the eclipsing region (star plus inner wind) can not be much larger than $1.2R_{\rm Roche,secondary}$.
– The size of the X-ray eclipsing region can be significantly larger than the size of the star due to absorption in the inner stellar wind. So one should be cautious in using this size as a measure of the true size of the Roche lobe of the secondary when evaluating the binary component mass ratio of SS433 from X-ray eclipse analysis.

Acknowledgements. Research has made use of data obtained from High Energy Astrophysics Science Archive Research Center Online Service, provided by the NASA/Goddard Space Flight Center. This work has been supported by RFBR grants N 04-02-16349, N 05-02-19710, N 06-02-16025, N 04-02-17276 and N 04-02-16720, and by joint RFBR/JSPS grant N 05-02-12710.

References

Abramowicz, M., 2004, astro, arXiv:astro-ph/0411185
Achmad, L., Lamers H.J.G.L.M., & Pasquini, L. 1997, A&A, 320, 196
Antokhina, É. A., Seifina, E. V., & Cherepashchuk, A. M. 1992, Soviet Astronomy, 36, 143
Barnes A., Casares P., **Charies J. et al., 2005, astro, arXiv:astro-ph/0501516**
Barnes, A. D. et al. 2006, MNRAS, 365, 296
Brinkmann W., Kawai N., Matsuoka M., Fink H. H., 1991, A&A, 241, 112
Cherepaschuk, A. 2002, Space Sci. Rev. 102, 23

Cherepashchuk, A. M., Sunyaev, R. A., Seifina, E. V. et al. 2003, A&A, 411, L441
Cherepashchuk A. M., et al., 2005, A&A, 437, 561
Dolan, J. F., et al. 1997, A&A, 327, 648
Eggleton, P. P., 1983, ApJ, 268, 368
Fabrika S. N., 1997, Ap&SS, 252, 439
Fabrika S. N., Goranskij V. P., Rakhimov V. Y., Panferov A. A., Bychkova L. V., Irsmambetova T. R., Shugarov S. Y., Borisov G. V., 1997, BSAO, 43, 109
Fabrika, S. 2004, Astrophysics and Space Physics Reviews, 12, 1
Gies, D. R., Huang, W., & McSwain, M. V. 2002, ApJ, 578, L67
Gies, D. R.; McSwain, M. V.; Riddle, R. L.; Wang, Z.; Wiita, P. J. & Wingert D. W. 2002, ApJ, 566, 1069
Hillwig, T. C., Gies, D. R., Huang, W., McSwain, M. V., Stark, M. A., van der Meer, A., & Kaper, L. 2004, ApJ, 615, 422
Kawai, N., Matsuoka, M., Pan, H., & Stewart, G. C. 1989, PASJ, 41, 491
Kotani, T., Kawai, N., Matsuoka, M. and Brinkmann, W. 1996, PASJ, 48, 619
Koval', E. & Shakura N., 1989, in Proc. 23rd ESLAB Symp. on Two- Topics in X-ray Astronomy (ESA SP-296), 479
Margon, B. 1984, ARAA, 22, 507.
Marshall, F. E., Swank, J. H., Boldt, E. A., Holt, S. S., & Serlemitsos, P. J. 1979, ApJ, 230, L1
Marshall, H. L., Canizares, C. R., & Schulz, N. S. 2002, ApJ, 564, 941
Matsuoka M., Takano S., Makishima K., 1986, MNRAS, 222, 605
Namiki, M., Kawai, N., Kotani, T., & Makishima, K. 2003, PASJ, 55, 281
Nandi A., Chakrabarti S., Belloni T., Goldoni P. 2005, MNRAS, 359, 629
Nazarenko V. V., Glazunova L. V., 2005, ARep, 49, 826
Okuda T., Teresi V., Toscano E. & Molteni D. 2005, MNRAS, 357, 295
Paczynski B., 1977, ApJ, 216, 822
Revnivtsev M., et al., 2005, A&A, 447, 545
Stewart G. C., et al., 1987, MNRAS, 228, 293
Watson M., S tewart G., Brinkmann W. , King A. 1986, MNRAS, 222, 261
Yuan, W., Kawai, N., Brinkmann, W., & Matsuoka, M. 1995, A&A, 297, 451